Supplemental Information

Topographic Mapping of the Synaptic Cleft into Adhesive Nanodomains

Karen Perez de Arce, Nikolas Schrod, Sarah W. R. Metzbower, Edward Allgeyer, Geoffrey K.-W. Kong, Aihui Tang, Alexander J. Krupp, Valentin Stein, Xinran Liu, Jörg Bewersdorf, Thomas A. Blanpied, Vladan Lucic, and Thomas Biederer

SUPPLEMENTAL DATA

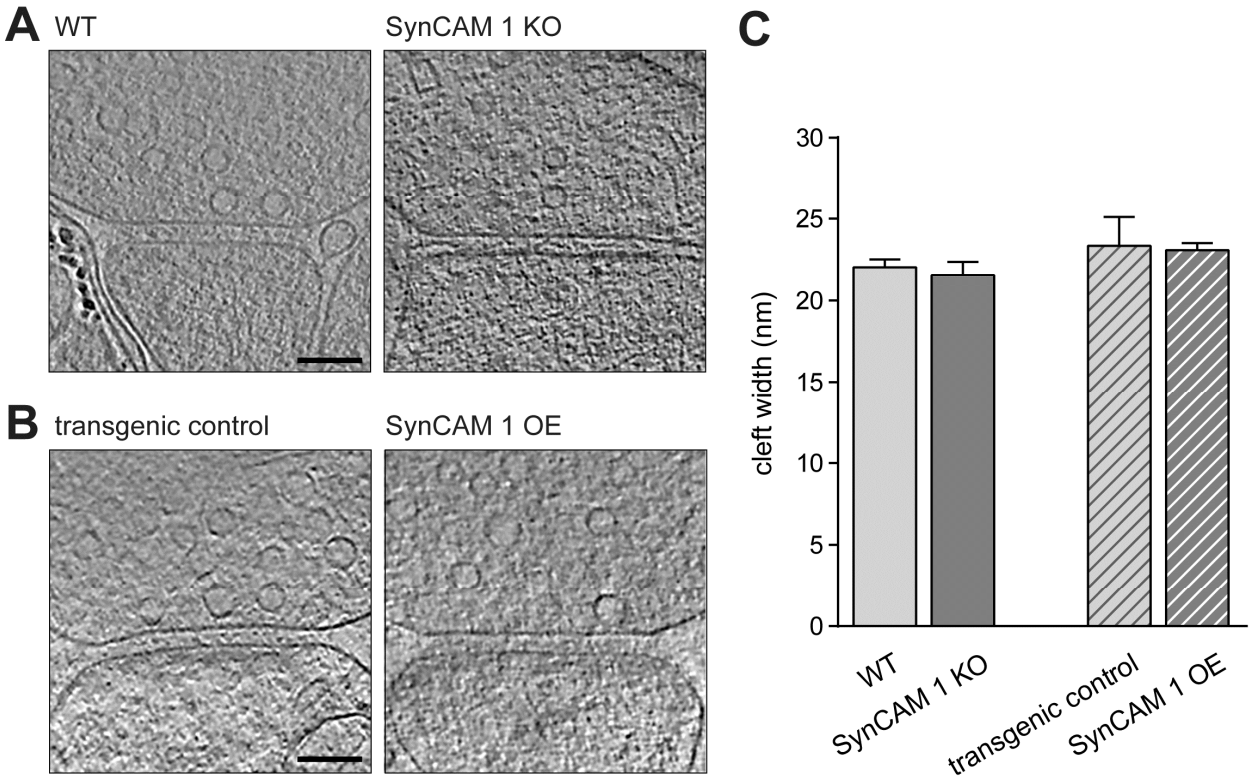

Supplemental Figure S1, related to Figure 1. Cryo-ET imaging and cleft width measurement.

(A) Representative images from tomograms of WT (left) and SynCAM 1 KO (right) synaptosomes. Tomogram data are shown at a depth of 2 voxels (4.6 nm). Scale bar, 100 nm. Note that panels in Figure 2D show tomograms at a depth of 4 voxels to add densities and better visualize cleft differences.

(B) Representative images from tomograms of transgenic control (left) and SynCAM 1 OE (right) synaptosomes. Tomogram data are shown at a depth of 2 voxels (5.5 nm). Scale bar, 100 nm.

(C) Cleft widths were measured in tomograms of synaptosomes from the indicated mouse lines. SynCAM 1 loss in KO mice or overexpression in OE mice did not affect cleft width as compared to littermate controls and across groups (n=7 WT synapses, 8 KO, 5 OE controls, 5 OE).

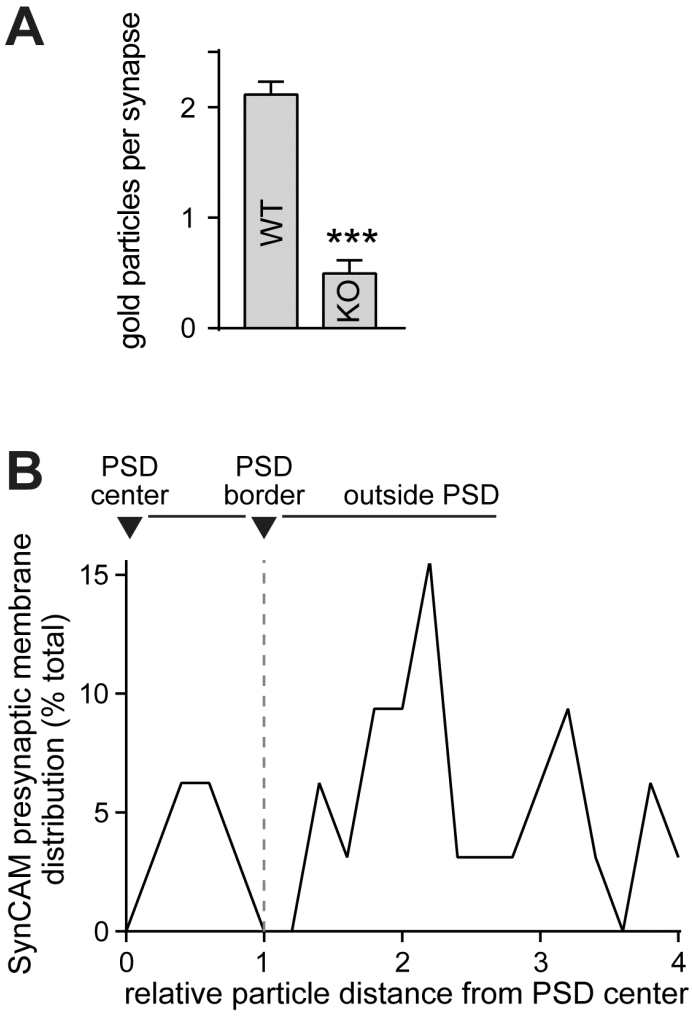

Supplemental Figure S2, related to Figure 2. Specificity of SynCAM 1 immuno-EM detection and protein distribution in presynaptic membranes.

(A) Quantification of gold particles per asymmetric synapse from WT and SynCAM 1 KO sections imaged as in Figure 2A shows specific SynCAM 1 immunolabeling (Mann-Whitney test, $p<0.0001$; N=44 micrographs each).

(B) Distribution of SynCAM 1 particles detected in presynaptic membranes. For each analyzed asymmetric synapse, presynaptic SynCAM 1 particle distances were measured relative to the center of the PSD and normalized to the PSD radius as depicted in Figure 2C, with a value of 1 corresponding to the PSD radius (n=97 micrographs from 3 mice).

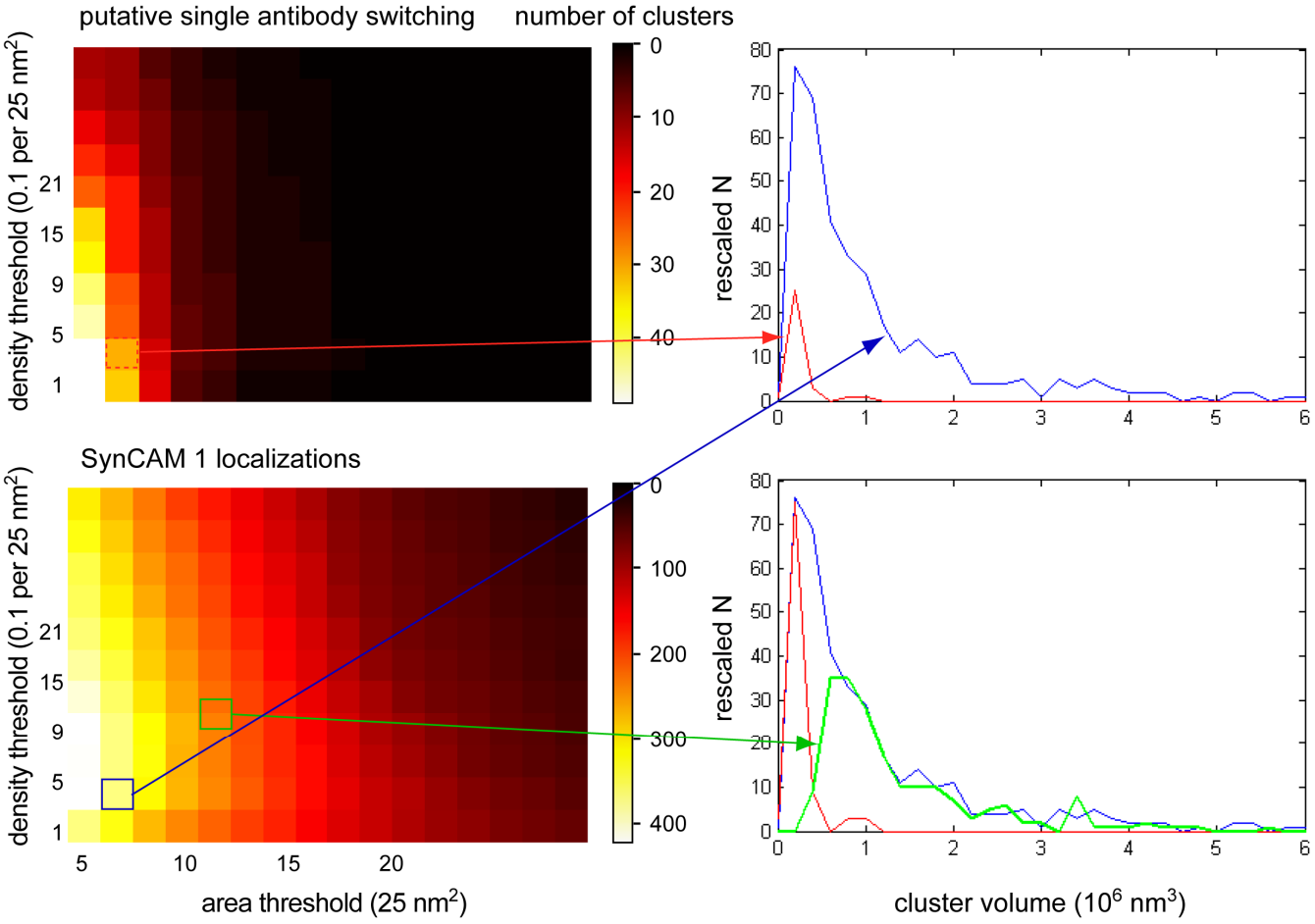

Supplemental Figure S3, related to Figure 3. Approach to identify the borders of SynCAM 1 ensembles.

To develop appropriate criteria for the analysis in Figure 3E, we compared the number of clusters detected with varying thresholds for density and area in each plane (x-y, x-z, and y-z) for the SynCAM 1 STORM data and for PSD-95 staining over a field with no synapses, where all localizations likely arise from repetitive switching of single molecules. In a reconstructed x-y distribution map with a pixel size of 5 nm, at relatively low density and area thresholds (0.3 localizations per pixel and 6 pixels, respectively), there was significant overlap in the distribution of cluster volumes between the SynCAM 1 data and the single molecule data. However, when thresholds were raised to 1 localization per pixel and an area of 10 pixels, single molecule clusters were no longer detected and the distribution of cluster volumes in the SynCAM data showed little overlap with the single molecule cluster volumes detected at the lower threshold (Figure 3E). This suggests that the clusters of SynCAM 1 we measure with these criteria are molecule assemblies of clustered molecules rather than artifacts of imaging or immunostaining.

Supplemental Media File 1, related to Figure 1. 3D cleft representation from a segmented tomogram.
The animation was generated with the Amira program for a 3D representation of the segmented tomogram shown in Figure 1A.

Supplemental Media File 2, related to Figure 1. Composite of a segmented tomogram.
Automated segmentation of a synaptic cleft is shown in red, highlighting the central density closer to the postsynaptic membrane.

SUPPLEMENTAL EXPERIMENTAL PROCEDURES

Synaptosome preparation and vitrification for tomography. Tomography experiments were performed with synaptosomes from SynCAM 1 KO mice (Fujita et al., 2006) generously provided by Dr. T. Momoi (National Institute for Neuroscience, Tokyo) and WT littermate controls in a mixed BL6/129Sv background. In addition, we analyzed SynCAM 1 overexpressor mice carrying the CaMKII-tTA (+/-) x TRE-SynCAM 1 (+/-) transgenes (Robbins et al., 2010) and used single-transgenic CaMKII-tTA (+/-) littermates as controls. These transgenic mice were in a hybrid SV129/Bl6 background. Synaptosomes were prepared as previously described (Dunkley et al., 1988; Godino Mdel et al., 2007). All steps were carried out at 4 °C. Briefly, male mice were sacrificed at 6-9 weeks of age, and the cerebral cortex was extracted and homogenized in ice-cold homogenization buffer (HB; 320 mM sucrose, 50 mM EDTA, 10 mM HEPES at pH 7.4) with up to seven strokes at 700 rpm in a Teflon-glass homogenizer. The homogenate was centrifuged for 2 min at 2,000 × g, the supernatant was centrifuged for 12 min at 9,500 × g, and the resulting pellet was resuspended in HB and loaded onto a three-step (3%, 10%, 23%) Percoll gradient (GE Healthcare). The gradients were spun for 6 min at 25,000 × g, the material accumulated at the 10%/23% interface was recovered and diluted to a final volume of 50 ml in HEPES-buffered medium (HBM, in mM: 140 NaCl, 5 KCl, 5 $NaHCO_3$, 1.2 Na_2HPO_4, 1 $MgCl_2$, 10 glucose, 10 HEPES [pH 7.4]). Percoll was removed by centrifugation for 10 min at 22,000 × g, and the pellet was resuspended in HBM supplemented with 1.2 mM $CaCl_2$. Synaptosomes were vitrified immediately after preparation by plunge-freezing as described (Fernandez-Busnadiego et al., 2013). Briefly, 3 μl of a synaptosomal suspension was placed onto a holey carbon copper electron microscopy grid (Quantifoil) that had been coated with BSA colloidal gold and plunged into a liquid ethane/propane mixture.

Tomographic acquisition, reconstruction and denoising. Tilt series were collected under a low dose acquisition scheme using an electron microscope (Polara; FEI) operated at 300 kV. The microscope was equipped with a field emission gun, a 2,048 × 2,048 charge-coupled device camera (MultiScan; Gatan), a postcolumn energy filter (Gatan) operated in the zero-loss mode, and a computerized cryostage designed to maintain the specimen temperature below -150 °C. Tilt series were recorded using Xplore3D (FEI), typically from -60° to 60° with 1.25°-1.5° angular increment. Pixel size was 0.58-68 nm at the specimen level, and the underfocus was set to 6-7 μm. Tilt series were aligned using gold beads as fiducial markers. 3D reconstructions were obtained by weighted backprojection using EM software (Hegerl, 1996), and tomograms were denoised by anisotropic non-linear diffusion (Fernández and Li, 2003). Tomograms that were not technically good (due to bad alignment or very low signal-to-noise

ratio) as well as those that did not show good structure preservation expected for cryo-preparation (smooth membranes, non-extracted cytosol) were discarded, resulting in total 5-8 tomograms from two mice for each genetic condition. Pre- and post-synaptic membranes were manually segmented in the Amira program. The cleft region was defined as the extracellular region between the membranes that spread as long as the pre- and post-synaptic membranes were parallel to each other. Radial regions (columns) were defined as concentric columns based on the relative position between the center (set to 0) and the cleft edge (set to 1) with bin values of 0, 0.25, 0.5, 0.75 and 1. Four cleft layers were determined by separating the cleft region into four layers of equal thickness parallel to the synaptic membranes. Additional layers of the same thickness were placed on the pre- and post-synaptic membranes to obtain values for normalization. This division into four layers and columns was our resolution limit to detect density differences. Due to the separation into four evenly spaced concentric columns, the outermost column contains approximately the same number of voxels as the inner three.

Tomogram greyscale values are directly related to electron density of the sample, where lower greyscale values correspond to higher densities. To analyze layer profiles, mean greyscale values of all layers in the cleft or for the layers of individual columns were calculated by first finding the individual mean greyscale value of each layer for each synapse, followed by averaging over all synapses of the genetic condition. In the same way, the standard deviation and the standard error of the mean were calculated from the individual means. In order to reduce the greyscale variability between tomograms, the values were shifted so that the mean density of synaptic membranes was set to 0 (Figure 1 E, H). To allow quantitative assessment of differences between layers and columns and the statistical analysis of these differences between genetic conditions, greyscale variability between tomograms arising from the acquisition and reconstruction procedures needed to be eliminated. To achieve this, greyscale values were normalized so that the mean density of synaptic membranes was set to 0 and the mean cleft density to 1 (Figure 1 F, J). This procedure reduces the difference between total cleft values of different tomograms because it leads to an increase of the greyscale values of synapses that contain above-average amount of proteins in the cleft and a decrease for synapses containing below-average amounts. There were no significant differences in synapse size and cleft width between the genetic conditions (Figure S1C). Cleft segmentation was performed using the thresholding and connectivity approach (Lucic et al., 2005). Specifically, clefts were initially segmented by thresholding at a conservative greyscale level and then only the segments that contact both pre- and postsynaptic membranes (in 3D) were selected. Greyscale calculations and the segmentation were done using custom-made software written in Python programming language that uses Numpy and Scipy packages (Oliphant, 2007).

High pressure tissue freezing and immuno-EM labeling. Experiments were performed with tissue from WT and SynCAM 1 KO littermate mice (Fujita et al., 2006) backcrossed for more than 10 generations in a C57Bl/6 background. Because standard pre-embedding immunogold EM did not yield sufficient labeling for quantitative analysis in our studies (data not shown), we employed high-pressure freezing, which improves preservation of proteins on lipids to yield better morphology and higher labeling density (Lonsdale et al., 1999). Acute hippocampal slices were prepared from 3-4 months old mice, allowed to recover for 2 h, and a 2 mm CA1 region was dissected. Unfixed samples were frozen using a Leica HMP101 at 2000 psi and controlled cryoprotecting conditions. Vitrified samples were freeze-substituted using a Leica EM AFS2 unit starting at -90 °C using 0.1% uranyl acetate and 0.125% glutaraldehyde in acetone for 50 hours, rinsed in 100% acetone and infiltrated over 10 hours at -60°C with Lowicryl HM20 resin (Electron Microscopy Science). Samples were placed in gelatin capsules and UV hardened at -50 °C for 8 hours. Blocks were then cut using a Leica UltraCut UC7. 60 nm sections were collected on formvar/carbon coated nickel grids and contrast stained using 2% uranyl acetate and lead citrate.

For immunodetection, the grids were placed section-side down on drops of 0.1 M ammonium chloride to quench untreated aldehyde groups, then blocked for nonspecific binding on 3% albumin from bovine serum (Sigma-Aldrich) in PBS. Single labeled grids were incubated overnight at 4°C on a primary anti-SynCAM 1 monoclonal antibody raised in chicken (MBL Laboratories, clone 3E1; 1:50), then bridged for 1 h at RT using rabbit anti-chicken antibodies (Jackson ImmunoResearch) at 1:200, and then incubated for 1 h at RT on anti-rabbit antibody-conjugated 10 nm Protein A gold (10 nm; Utrecht Medical Center) at 1:50. All antibodies and Protein A gold were diluted in PBS containing 3% BSA. The grids were rinsed with PBS, fixed using 1% glutaraldehyde for 5 min, rinsed again, and transferred to a UA/methylcellulose drop before being collected and dried. Grids were observed using a FEI Tecnai Biotwin transmission electron microscope at 80kV accelerating voltage, and images were taken using a SIS Morada CCD camera and iTEM (Olympus) software.

Our post-embedding staining of thin EM sections is expected to allow for uniform antibody access at both the edge and the center of synapses, and access issues are unlikely to cause a detection bias. For quantification of SynCAM 1 distribution across synaptic compartments, presynaptic membranes and terminals were identified by presence of synaptic vesicles within the terminal, and postsynaptic membrane identified due to their association with an electron-dense region. Immunogold particles were only scored as labeling SynCAM 1 in pre- or post-synaptic membranes if particles were within 40 nm of the membrane, using the diameter of the gold particles to approximate this distance. In the few cases when particles were observed within 30 nm from the pre- and post-synaptic membrane, those gold

particles were excluded. Note that the full extracellular domain of a SynCAM dimer has a predicted length of 26-28 nm, assuming that the extracellular domains are rigid and project towards each other (Y. Modis, pers. comm.), and only a small fraction of presynaptic SynCAM 1 closer to the active zone border may connect to SynCAM 1 at the postsynaptic edge.

Neuronal cultures. For STORM analysis, hippocampal neurons were cultured from E18 rat embryos as described (Frost et al., 2010) and plated on cover glasses (MacGillavry et al., 2013).

For confocal microscopy co-localization analysis, hippocampal neurons were prepared from rats at E18 as described (Kaech and Banker, 2006) with modifications. In brief, dissected hippocampi were incubated in 0.05% trypsin at 37 °C for 20 minutes (Invitrogen 25300054) and plated at a density of ~30,000 cells per coverslip. Dissociated cells were plated on poly-l-lysine (Sigma P1274) and incubated in a cell culture incubator with 5.0% CO2. Cytosine arabinoside (Sigma C1768) was added at a final concentration of 2 μM per well 2 days in vitro to prevent glia cell overgrowth.

For confocal microscopy analysis after chemical LTD, primary hippocampal neurons were dissected from rats at P1 as described (Biederer and Scheiffele, 2007) and plated on Matrigel (Becton-Dickinson Biosciences). Chemical LTD was induced by treating neurons at 14 div for 3 min with 20 μM NMDA (Ehlers, 2000; Lee et al., 1998). Medium was then rapidly exchanged, and cultures were incubated for 60 min prior to labeling of surface SynCAM 1 and staining for PSD-95 as described below.

Immunostaining of dissociated neurons for confocal analysis. To measure the extent of triple co-localization of SynCAM 1 and EphB2 together with Homer, surface labeling of EphB2 and SynCAM 1 was performed in neurons at 14 div. Cells were incubated in cold PBS for 3 min to restrict trafficking, followed by 10 min incubation with chicken monoclonal anti-SynCAM 1 (MBL Laboratories, clone 3E1; 1:1000) or goat anti-EphB2 (R&D Systems, AF467; 1:100) antibodies against the extracellular domain in PBS. Neurons were kept on ice during antibody surface labeling. After two washes with ice-cold PBS and fixation for 15 min with cold 4% PFA / 4% sucrose in PBS, cells were blocked with 5% FBS in PBS for 1 h at RT, and incubated for 1 h at RT with secondary Alexa-conjugated antibodies (Invitrogen; 1:1000). After washes, cells were permeabilized with 0.1% Triton-X100 in PBS for 10 min at RT, and processed for scaffold protein immunostaining. Homer was detected with antibodies raised in rabbits (Synaptic Systems, 160 003; 1:2000). Mouse monoclonal antibodies detected PSD-95 (NeuroMab, clone K28/43; 1:500). Incubations with secondary Alexa-conjugated antibodies (Invitrogen; 1:1000) were for 1 h at RT. Coverslips were mounted on Aqua-Mount mounting media (Thermo Scientific).

STED imaging. For STED microscopy, hippocampal neurons were prepared from rats at P1 as described (Biederer and Scheiffele, 2007) and plated on 12 mm coverslips #1.5 (Glaswarenfabrik Karl Hecht GmbH&Co KG). At 14 div, SynCAM 1 and EphB2 primary antibody staining was performed under trafficking restrictive conditions as described above. For SynCAM 1, primary antibody surface labeling was followed by incubation with rabbit anti-chicken IgY as bridge antibody (EMD Millipore, 12-334; 1:10,000) for 3 h at 4 °C. After washes, labeling with goat anti-rabbit IgG antibodies conjugated with ATTO-647N (Active Motif, Carlsbad, CA, 15068; 1:500) was performed for 1 h at RT. This was followed by permeabilization and staining for PSD-95 as described above, and detection was performed with goat anti-mouse IgG antibodies (Sigma, 76085; 1:500) labeled with ATTO-594 (ATTO-TEC) for 1 h at RT. For STED microcopy of EphB2, primary antibody labeling was followed by washes and incubation with rabbit anti-goat IgG conjugated with ATTO594 (Abgent, San Diego, CA, ASR1144; 1:250) for 1 h at RT, and extensively washed. This was followed by permeabilization and staining for Homer as described above, and detection was performed with goat anti-rabbit IgG antibodies (Active Motif, Carlsbad, CA, 15068; 1:500) labeled with ATTO-647N (ATTO-TEC) for 1 h at RT. To avoid cross-detection, coverslips were washed extensively after labeling of EphB2 with secondary antibodies prior to Homer detection, and non-overlapping signals were confirmed by confocal and STED microscopy. Coverslips were mounted on Mowiol (Sigma, 81381).

Imaging was performed on a custom built gated detection, beam scanning, all pulsed laser STED system. ATTO-647N conjugated secondary antibodies were imaged by focusing approximately 30 µW (at the back aperture) of picosecond pulsed 650 nm laser light (LDH-P-C-650, Picoquant) into the back aperture of a 100X oil immersion objective lens (UPLAPO 100XO/PSF, Olympus) to excite fluorescence. Similarly, ATTO-594 conjugated secondary antibodies were excited with approximately 35 µW of picosecond pulsed 595 nm excitation light (LDH-TA-595, Picoquant). Fluorescence in the periphery of the excitation spot was depleted with approximately 200 mW of 600 picosecond pulsed 775 nm light (Katana HP, One Five). The depletion light was imprinted with a 2pi phase ramp using a spatial light modulator (X10468, Hamamatsu) and then circularly polarized with a quarter wave plate. Both the depletion and excitation beams were scanned through the sample using a 16 kHz resonant mirror (SC-30, Electro-Optical Products Corp.) and galvanometer mirror pair (DynAXIS XS, ScanLab) conjugated to the objective back pupil plane. Fluorescence was collected by the same objective and separated from the excitation/depletion beam path with a custom dichroic mirror (zt485/595/640/775rpc, Chroma). A second dichroic mirror (zt640rdc, Chroma) separated the ATTO-647N channel from the ATTO-594 channel and each channel employed a set of band pass filters (FF01-685/40 and FF01-624/40, Semrock).

For each channel, fluorescence was focused into a multimode fiber corresponding to approximately 0.8 airy units acting as the confocal pinhole. Finally, fluorescence was detected by a single photon counting avalanche photodiode (SPCM-ARQ-13-FC, Perkin Elmer), collected by an FPGA based data acquisition card (PCIe-7852R, National Instruments), and transferred to a host computer. The excitation and depletion lasers were synchronized with custom electronics (Opsero Electronics) that also hardware gated both detector's signals for gated detection. All images were collected at 10 nm pixel size.

STED image analysis. Image analysis was performed with custom Matlab (Mathworks) scripts. SynCAM 1 or EphB2 spot locations were determined by fitting with a two-dimensional Lorentzian function and their fitted center positions and widths were stored. The corresponding PSD-95 and Homer images, respectively, were analyzed by first lightly blurring with a 1 pixel sigma Gaussian and then setting a threshold of two standard deviations above the mean for all nonzero pixels. This threshold was applied to the original image and size of the remaining regions was examined. Only the top two percent largest regions were retained and their boundaries were determined. In this way, PSD-95 and Homer regions were determined based on size and brightness. Finally, the distance between the center position of each SynCAM 1 spot and the nearest PSD-95 boundary was found. Distances pf EphB2 spots and the nearest Homer boundary were determined in the same way. If a SynCAM 1 or EphB2 spot was found inside a PSD region, the PSD boundary distance was marked as negative. The script is available upon request.

2-Color 3D STORM imaging. Surface labeling of SynCAM 1 and EphB2 followed by staining of intracellular Homer was performed as described above in hippocampal neurons cultured from E18 rats on div 12-14. Secondary anti-chicken antibodies against SynCAM 1 or EphB2, and anti-rabbit antibodies against Homer were conjugated to Cy3 and Alexa 647, respectively. Imaging was performed on an Olympus IX81 ZDC2 inverted microscope with a 100X/1.49 TIRF oil immersion objective. Fluorophores were excited with semi-oblique illumination from 647 nm (100 mW) and 561 nm (150 mW) lasers simultaneously. Stochastic blinking of both molecules was detected with an iXon+ 897 EM-CCD camera (Andor) placed after a 1.6x magnifying optic and a DV2 chromatic image splitter (Photometrics). Frames were acquired at 50 Hz; excitation was pulsed to last 10 ms per frame. A total of 15,000 to 30,000 frames were collected. Hardware was controlled via iQ software (Andor). Z stability was maintained by the Olympus ZDC2 feedback positioning system. An astigmatic lens (f=300 mm) was added to each emission filter holder in the DV2 and the Z-axis positions of localized molecules were deduced post hoc essentially as described (Dani et al., 2010; Huang et al., 2008).

2-Color 3D STORM analysis. All analyses were performed using custom MATLAB (Mathworks) scripts. Molecular positions in the XY plane were estimated by fitting the detected fluorescence peaks with an elliptical 2-D Gaussian function, and Z position was deduced from calibrations of astigmatism above and below the focal plane (Huang et al., 2008; van de Linde et al., 2011). Poorly localized molecules were rejected from the analysis. PSDs were identified based on the density map of Homer localizations analyzed sequentially in the x-y, x-z and y-z planes. Only those clusters that met both density and area criteria were identified as PSDs and used for further analysis. The average density of SynCAM 1 localizations was calculated within 25 nm radial bins from the PSD border by dividing the number of SynCAM 1 localizations by the bin volume. To exclude the effects of PSD shape and optical section restriction, the volume of each bin was deduced by counting the number of uniformly distributed localizations that appeared within it in simulations. The average SynCAM 1 density within the PSD was calculated by dividing the number of SynCAM 1 localizations within the PSD by the total PSD volume defined by Homer localizations. The script is available upon request.

Confocal microscopy and analysis. Confocal imaging was performed on a Leica TCS SPE DM2500 microscope equipped with one spectral PMT. Fluorochromes imaged include Alexa 488, Alexa 594, and Alexa 647 (Invitrogen). Unless otherwise stated, images were acquired with an ACS APO 63x oil lens with 1.3 numerical aperture, using same settings for each condition. The neurite segments that were selected for analysis were between 20-60 μm long. Images were analyzed with ImageJ using scripts custom-written by Ding Lai; Harvard NeuroDiscovery Center Enhanced Neuroimaging Core, Harvard Medical School). The first script measures the extent of immunostaining signal overlap in three channels to determine dual and triple co-localization. The second custom written script measures the area of SynCAM 1 puncta and their distance to the center of the nearest PSD-95 punctum. The scripts are available upon request.

Data and statistical analyses. Data analysis was performed using GraphPad Prism 5 (Graph Pad Software, La Jolla, USA) and MATLAB (Mathworks). * denotes t-test $p<0.05$; ** $p<0.01$; *** $p<0.001$. Data in the text are reported as average ± standard error of the mean. t-tests were unpaired unless noted otherwise in the text.

Animal procedures. All animal procedures undertaken in this study were approved by the Institutional Animal Care and Use Committees and were in compliance with NIH guidelines.

SUPPLEMENTAL REFERENCES

Biederer, T., and Scheiffele, P. (2007). Mixed-culture assays for analyzing neuronal synapse formation. Nature Protocols 2, 670-676.

Dani, A., Huang, B., Bergan, J., Dulac, C., and Zhuang, X. (2010). Superresolution imaging of chemical synapses in the brain. Neuron 68, 843-856.

Dunkley, P.R., Heath, J.W., Harrison, S.M., Jarvie, P.E., Glenfield, P.J., and Rostas, J.A. (1988). A rapid Percoll gradient procedure for isolation of synaptosomes directly from an S1 fraction: homogeneity and morphology of subcellular fractions. Brain Res 441, 59-71.

Ehlers, M.D. (2000). Reinsertion or degradation of AMPA receptors determined by activity-dependent endocytic sorting. Neuron 28, 511-525.

Fernandez-Busnadiego, R., Asano, S., Oprisoreanu, A.M., Sakata, E., Doengi, M., Kochovski, Z., Zurner, M., Stein, V., Schoch, S., Baumeister, W., and Lucic, V. (2013). Cryo-electron tomography reveals a critical role of RIM1alpha in synaptic vesicle tethering. J Cell Biol 201, 725-740.

Fernández, J.J., and Li, S. (2003). An improved algorithm for anisotropic nonlinear diffusion for denoising cryo-tomograms. J Struct Biol 144, 152-161.

Frost, N.A., Shroff, H., Kong, H., Betzig, E., and Blanpied, T.A. (2010). Single-molecule discrimination of discrete perisynaptic and distributed sites of actin filament assembly within dendritic spines. Neuron 67, 86-99.

Fujita, E., Kouroku, Y., Ozeki, S., Tanabe, Y., Toyama, Y., Maekawa, M., Kojima, N., Senoo, H., Toshimori, K., and Momoi, T. (2006). Oligo-astheno-teratozoospermia in mice lacking RA175/TSLC1/SynCAM/ IGSF4A, a cell adhesion molecule in the immunoglobulin superfamily. Mol Cell Biol 26, 718-726.

Godino Mdel, C., Torres, M., and Sanchez-Prieto, J. (2007). CB1 receptors diminish both Ca(2+) influx and glutamate release through two different mechanisms active in distinct populations of cerebrocortical nerve terminals. J Neurochem 101, 1471-1482.

Hegerl, R. (1996). The EM program package: A platform for image processing in biological electron microscopy. J Struct Biol 116, 30-34.

Huang, B., Wang, W., Bates, M., and Zhuang, X. (2008). Three-dimensional super-resolution imaging by stochastic optical reconstruction microscopy. Science 319, 810-813.

Kaech, S., and Banker, G. (2006). Culturing hippocampal neurons. Nat Protoc 1, 2406-2415.

Lee, H.K., Kameyama, K., Huganir, R.L., and Bear, M.F. (1998). NMDA induces long-term synaptic depression and dephosphorylation of the GluR1 subunit of AMPA receptors in hippocampus. Neuron 21, 1151-1162.

Lonsdale, J.E., McDonald, K.L., and Jone, R.L. (1999). High pressure freezing and freeze substitution reveal new aspects of fine structure and maintain protein antigenicity in barley aleurone cells. The Plant Journal 17, 221-229.

Lucic, V., Forster, F., and Baumeister, W. (2005). Structural studies by electron tomography: from cells to molecules. Annu Rev Biochem 74, 833-865.

MacGillavry, H.D., Song, Y., Raghavachari, S., and Blanpied, T.A. (2013). Nanoscale scaffolding domains within the postsynaptic density concentrate synaptic AMPA receptors. Neuron 78, 615-622.

Oliphant, T.E. (2007). Python for Scientific Computing. Comp Sci & Eng 9, 10-20.

Robbins, E.M., Krupp, A.J., Perez de Arce, K., Ghosh, A.K., Fogel, A.I., Boucard, A., Sudhof, T.C., Stein, V., and Biederer, T. (2010). SynCAM 1 adhesion dynamically regulates synapse number and impacts plasticity and learning. Neuron 68, 894-906.

van de Linde, S., Loschberger, A., Klein, T., Heidbreder, M., Wolter, S., Heilemann, M., and Sauer, M. (2011). Direct stochastic optical reconstruction microscopy with standard fluorescent probes. Nat Protoc 6, 991-1009.